Increased redox protein loading on carbon nanotube electrodes

Katherine E. Moore[†], **Benjamin S. Flavel**[‡], **Jingxian Yu**[§], **Andrew D. Abell**[§], **Joseph G. Shapter**[†]*

[†]**Flinders Centre for Nanoscale Science and Technology, Flinders University, Sturt Road, Bedford Park, Adelaide 5000, South Australia**

[‡]**Institute of Nanotechnology, Karlsruhe Institute of Technology D-76021 Karlsruhe, Germany**

[§]**School of Chemistry and Physics, The University of Adelaide, Adelaide 5000, South Australia**

*Corresponding author e-mail address: joe.shapter@flinders.edu.au (J. G. Shapter)

Abstract

Carbon nanotube (CNT) electrodes for electrochemistry were fabricated from single- and double- walled carbon nanotubes. The electrodes were subsequently covalently loaded with a ferrocene modified α-aminoisobutyric acid protein, and tested by cyclic voltammetry. The CNT electrode comprised of double walled CNTs (DWCNTs) demonstrated significantly higher peak current (I_p) compared to their single walled counterparts (SWCNTs). This is attributed to a higher loading of the ferrocene modified protein to the outer wall of the nanotube, through the presence of a larger number of defects sites within the sp^2 carbon lattice for the DWCNTs. This higher loading was achieved without compromising the electron transfer rate, indicating that DWCNTs may offer a useful alternative to SWCNTs in future electrochemical sensors and biosensors.

Keywords: Double walled carbon nanotubes, cyclic volammetry, redox probe loading.

1. Introduction

Carbon nanotubes (CNTs) are a highly desirable material for incorporation into electrochemical [1-2] and biological sensing devices [3-4] owing to their fast heterogeneous electron transfer, high surface area and electrochemical stability [5-6]. Furthermore the conductivity of CNTs has been shown to be remarkably sensitive to changes in surface adsorbates, making them ideal for highly sensitive nanoscale sensors [7]. To date many different carbon nanotube based electrochemical sensors and biosensors exist in the literature, consisting of either randomly dispersed [8-9] or well-ordered nanotube arrays [6, 10-11]. However, in all cases the CNTs act as a molecular wire, allowing electrical communication between the underlying electrode and a redox species [7, 12]. For well ordered or vertically aligned CNT arrays, fast charge transfer has been demonstrated and is a significant advantage compared to randomly dispersed CNTs [5]. This has lead to the development of highly sensitive, reagentless sensing devices [7], where direct electron transfer between the active redox-centre and an electrode surface occurs without the need for mediators. Due to the presence of a large working surface area and easy access of an analyte to the immobilised sensing probe [6], well ordered or vertically aligned carbon nanotube electrodes have been loaded with molecular sensitive materials such as DNA [6, 13], Cu nanoparticles [14] and anti-immunoglobin G [11].

This has led to the detection of a wide range of analytes with improved sensitivity and selectivity [2]. For example, Gou *et al.* [13] recently reported a horizontally aligned CNT genosensor consisting of single-stranded DNA bridging a gap between SWCNTs, which was subsequently sensitive to complementary-stranded DNA. A well-matched DNA duplex was shown to exhibit resistance in the order of 1 MΩ, which in the presence of a GT or CA mis-match was increased ~300-fold. Somenath *et al.* also demonstrated a cholesterol sensor based upon modification of vertically aligned multi walled CNTs (MWCNTs) with the

biocompatible polymer, polyvinyl alcohol, decorated with cholesterol oxidase (ChOx) [15]. In this sensor the use of carbon nanotubes was found to significantly increase sensor sensitivity through increases in the signal to noise ratio, and was directly attributed to an increase in surface area allowing a high loading of ChOx. An almost linear relationship between cholesterol concentration and the response current was observed in a clinical range up to 300 mg dL^{-1}. Flavel *et al.* [16] also demonstrated a copper ion sensor fabricated from CNT arrays decorated with the tripeptide Gly-Gly-His, capable of detecting concentrations as low as 1 ± 6 μM. Additionally, Gooding and co-workers utilized vertically aligned glucose oxidase (GOx) modified SWCNTs on a cysteamine modified gold surface, demonstrating a GOx surface concentration of 52 x 10^{-9} mol cm^{-2} with apparent electron transfer rate of 9 s^{-1} [12]. Despite the high surface coverage of GOx, achieved by utilizing highly functionalized SWCNT, the poor apparent electron transfer rate indicates destruction of the carbon nanotubes' unique electronic property through the introduction of defects.

As detailed in a recent review from Diao and Liu [17], several methods exist to chemically assemble CNTs on electrode surfaces. However, common to each of methods is chemical functionalisation of the nanotubes, most commonly with carboxylic acid groups [18] and their subsequent covalent linking to a surface via an ester [19-20] or amide bond [12]. Unfortunately, such chemical functionalisation introduces defects in the hexagonally bonded sp^2 [21] lattice, which has the effect of disrupting many of the attractive properties of nanotubes, particularly charge transport [22]. We have recently shown that in order to avoid such disruption DWCNT are advantageous, whereby the outer tube can be selectively functionalized [23] with the inner tube retaining its undisrupted sp^2 network and hence it's intrinsic electronic properties. The ability to achieve this was then demonstrated in a comparison between carboxyl functionalised SWCNTs and DWCNTs immobilised on a self-assembled cysteamine layer on gold [24]. Electron transport was then isolated to the CNTs

by introduction of a polystyrene layer, filling the voids between CNT bundles, with DWCNTs showing a higher apparent electron transfer rate constants for diffusion limited redox with $Ru(NH_3)_6^{+3/2}$.

In this work the demonstrated benefits of utilising DWNTs are capitalised upon by covalently linking an electro-active ferrocene terminated α-aminoisobutyric acid protein (Aib_5-Fc), see Figure 1 (a), to vertically aligned arrays of DWCNTs on cysteamine modified gold substrates. As a further demonstration of the advantage of DWCNTs, an analog system is also fabricated for SWCNTs. It is shown that not only do DWCNTs have an improved redox protein loading, but also superior electron transfer kinetics compared to SWCNTs.

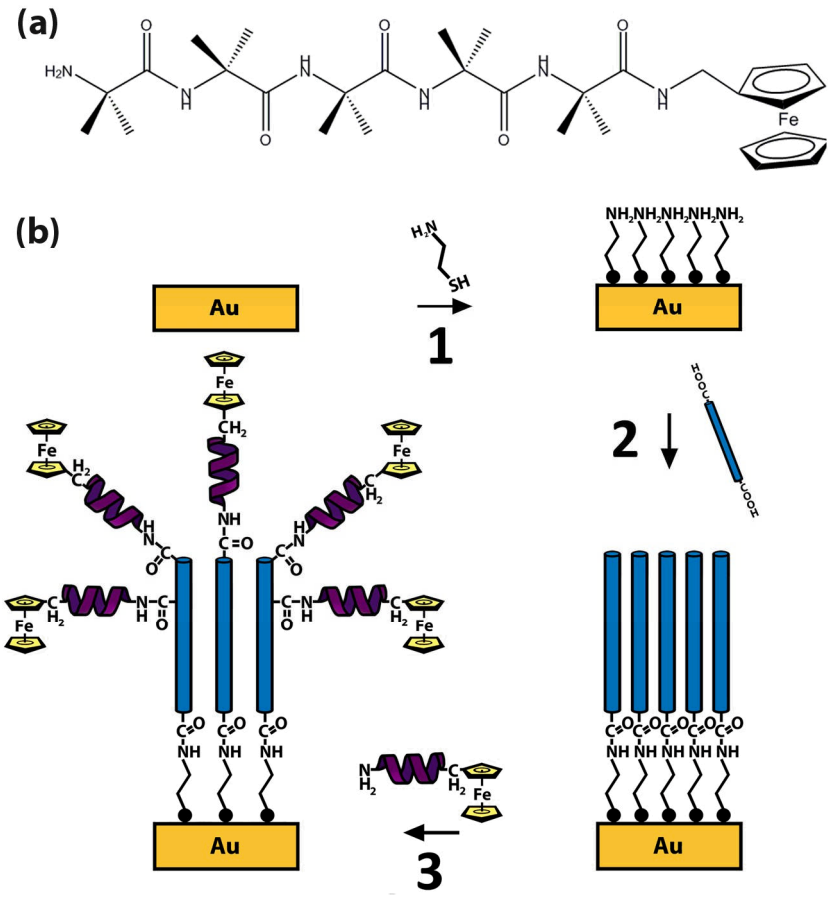

Figure 1 *(a) The redox protein Aib_5-Fc and (b) fabrication of CNT electrodes decorated with covalently bound redox proteins.*

2. Experimental

2. 1 Synthesis of Aib_5-Fc

Fmoc-Aib-OH loaded 2-chlorotrityl chloride resin (GL Biochem) was transferred into a sintered funnel. After the Fmoc group was removed by reaction with a solution of 25% piperidine (Merck) in N,N-dimethylformamide (DMF) (Merck) for 30 min, a solution of 0.05 M Fmoc-Aib-OH (GL Biochem Ltd) in DMF containing 0.2 M 2-(1H-7-azabenzotriazol-1-yl)-1,1,3,3-tetramethyl uronium hexafluorophosphate methanaminium (HATU) (GL Biochem

Ltd) and 0.2 M diisopropylethyl amine (DIPEA) (Sigma-Aldrich) was added to the deprotected resin. The mixture was left for 2 h with occasional stirring, and then the resin was isolated by filtration. Successive additions of Fmoc-Aib-OH were carried out, using this protocol, to yield H_2N-Aib_4-OH loaded resin. In the last cycle, Boc-Aib-OH was capped onto the resin using the same protocol. The oligopeptide was cleaved with 2% trifluoroacetic acid (TFA) (Sigma-Aldrich) / DCM (v/v). After purification by high-performance liquid chromatography (HPLC), the resulting peptide Boc-Aib_5-OH was added to a solution of 0.05 M ferrocenylmethylamine [25-26] in DMF containing 0.2 M HATU and 0.2 M DIPEA. With stirring for 24 h at room temperature, the product Boc-Aib_5-Fc was purified by HPLC and further treated by a 4 M HCl / dioxane solution for 15 min. After purification, the final H_2N-Aib_5-Fc was characterised by NMR and MS. ^{1}H NMR (300MHz, DMSO) δ 8.44 (s, 1H, NH), 8.07 (s, 1H, NH), 7.91 (s, 1H, NH), 7.76 (s, 1H, NH), 7.24 (s, 1H, NH), 4.27 (m, 2H), 4.21 (m, 5H, Cp), 4.17 (m, 2H), 4.05 (d, 2H, CH_2), 1.52 (s, 6H, 2 βCH_3), 1.33 (s, 6H, 2 βCH_3), 1.32 (s, 6H, 2 βCH_3), 1.25 (s, 6H, 2 βCH_3), 1.23 (s, 6H, 2 βCH_3); MS: $[M+Na]^-_{calcd}$ = 663.6, $[M+Na]^-_{found}$ = 663.5.

2.2 Preparation of Au/Cysteamine/CNT/Aib_5-Fc electrodes

DC arc discharge synthesized SWCNTs (Carbon Solutions Inc., P2-SWCNT, Diameter 1.4 – 1.6 nm, Length 0.5 – 1.5 μm) and CVD produced DWCNTs (Nanolab, Diameter 3 - 5 nm, Length 1 – 5 μm) were purchased and functionalized using previously reported methods [23]. CNTs were then suspended in a solution of dimethylsulfoxide (Sigma-Aldrich) containing 0.2 mg mL^{-1} CNTs, 0.25 mg mL^{-1} *N*,*N*'-dicyclohexylcarbodiimide (DCC) (Fluka) and 0.14 mg mL^{-1} dimethylaminopyridine (DMAP) (Sigma-Aldrich). Polished flat gold disk electrodes (2 mm diameter) were cleaned in 25 % v/v H_2O_2/ KOH (50 mM) for 20

min and then electrochemically cleaned by cycling between 0 and 1.5 V vs. Ag/AgCl in 50 mM KOH. This cleaning process yielded clean gold surfaces with peak separations of 59 mV for a (1 mM) $Ru(NH_3)_6^{+3/2}$ containing solution. The clean, flat surfaces were then incubated in cysteamine (Sigma-Aldrich) for 24 h resulting in exposed amine groups (Figure 1 (b), step 1). These substrates were then exposed to SWCNT or DWCNT solution for 24 h, after which they were rinsed with propan-2-ol (Merck) and dried under nitrogen (Figure 1 (b), step 2). The surfaces were then exposed to 0.01 M H_2N-Aib_5-Fc in DMF solution containing 0.5 M HATU and 0.5 M DIPEA for 48 h before being further rinsed and dried (Figure 1 (b), step 3).

2.3 Electrochemistry

All electrochemistry measurements were taken with a CH Instruments Electrochemical Analyser (CH Instruments Inc). The CNT modified gold surface formed the working electrode (geometric area of 0.33 cm^2), with platinum wire and Ag/AgCl used as the counter and reference electrodes, respectively. Cysteamine characterisation was conducted in 1 mM pH 6.5 potassium phosphate buffer. The peak area of the cysteamine oxidation peak was calculated by subtracting the second scan from the first. Surface area calculation was conducted in 1 mM ruthenium hexamine in potassium phosphate buffer pH 7.5 by cycling between 0.2V and -0.6V vs. Ag/AgCl/KCl (3 M), in the negative direction initially. CNT electrodes were electrochemically characterised in 1 mM tetrabutylammoniumhexafluorophosphate (TBAPF6) (Sigma-Aldrich) in acetonitrile at scan rates of 25 – 1000 mV s^{-1}. Due to the low concentration of surface redox species, these cyclic voltammograms have been background subtracted using the fityk software 0.8.6 (http://www.unipress.waw.pl/fityk/).

3. Results and Discussion

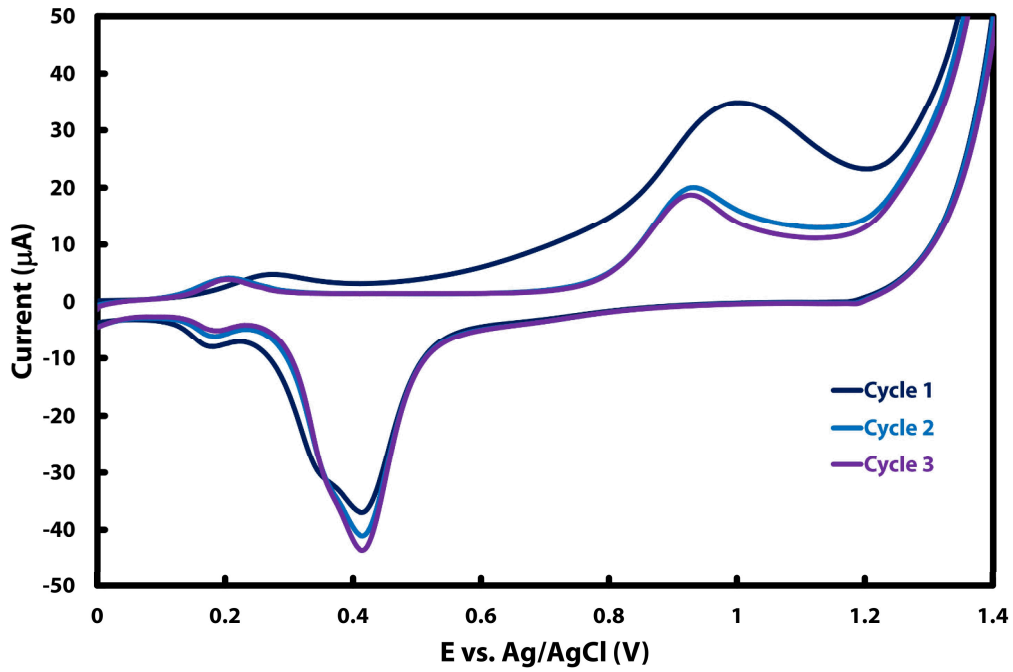

Figure 2 *Cyclic voltammetry cycle 1, 2 and 3 of a self assembled monolayer on polished gold in pH 6.5 potassium phosphate buffer, showing the irreversible oxidation of cysteamine at a scan rate of 100 mV* s^{-1}.

In order to determine the packing density of the cysteamine monolayer and thereby the availability of amine terminal groups for carbon nanotube attachment, the surface concentration of the cysteamine was calculated. Three self assembled monolayer (SAM) modified gold electrodes were cycled between 0 and 1.4 V by cyclic voltammetry in 1 mM pH 6.5 phosphate buffer against Ag/AgCl. Figure 2 shows the first three cycles at a scan rate of 100 mV/s. In the first cycle a large oxidation peak centred at 0.997 V can be seen, and is absent from subsequent scans. Additionally, peaks centred at 0.930 V and 0.460 V can be seen and correspond to the oxidation and reduction of gold, and remain approximately equal for subsequent cycles. This indicates that the gold-sulphur bond of the cysteamine is irreversibly oxidised during the first scan, resulting in complete removal of the SAM from the

gold surface. These observations are in excellent agreement with the literature [27-29] with the proposed mechanism for this reaction seen in Equation 1 [27].

$$AuS(CH_2)_2NH_2 + e^- \rightarrow Au(0) + {}^-S(CH_2)_2NH_2 \qquad E = +1.00\ V\ vs.\ Ag/AgCl \qquad (1)$$

Using the oxidation peak area, Laviron's theory [30] and the following equations, the average surface concentration of cysteamine was determined.

$$I_p = \frac{n^2F^2A\Gamma\upsilon}{4RT} = \frac{nFQ\upsilon}{4RT}$$

$$\Gamma_{cyst} = \frac{Q_{cyst}}{nFA}$$

where Γ is the surface concentration (mol cm^{-2}), A is the electro-active area (cm^2), Q is the peak area of the voltammogram (C), I_p is the peak current (A) and n is the number of electrons involved.

The resultant surface concentration of cysteamine was found to be $3.31 \pm 0.39 \times 10^{-8}$ mol cm^{-2}, and is significantly higher compared to previous work by Esplandiú *et al.* [28] who reported 4.66×10^{-9} mol cm^{-2}. This result suggests that a highly packed cysteamine layer was formed in this work and therefore a large number of surface amine sites for carbon nanotube attachment exist.

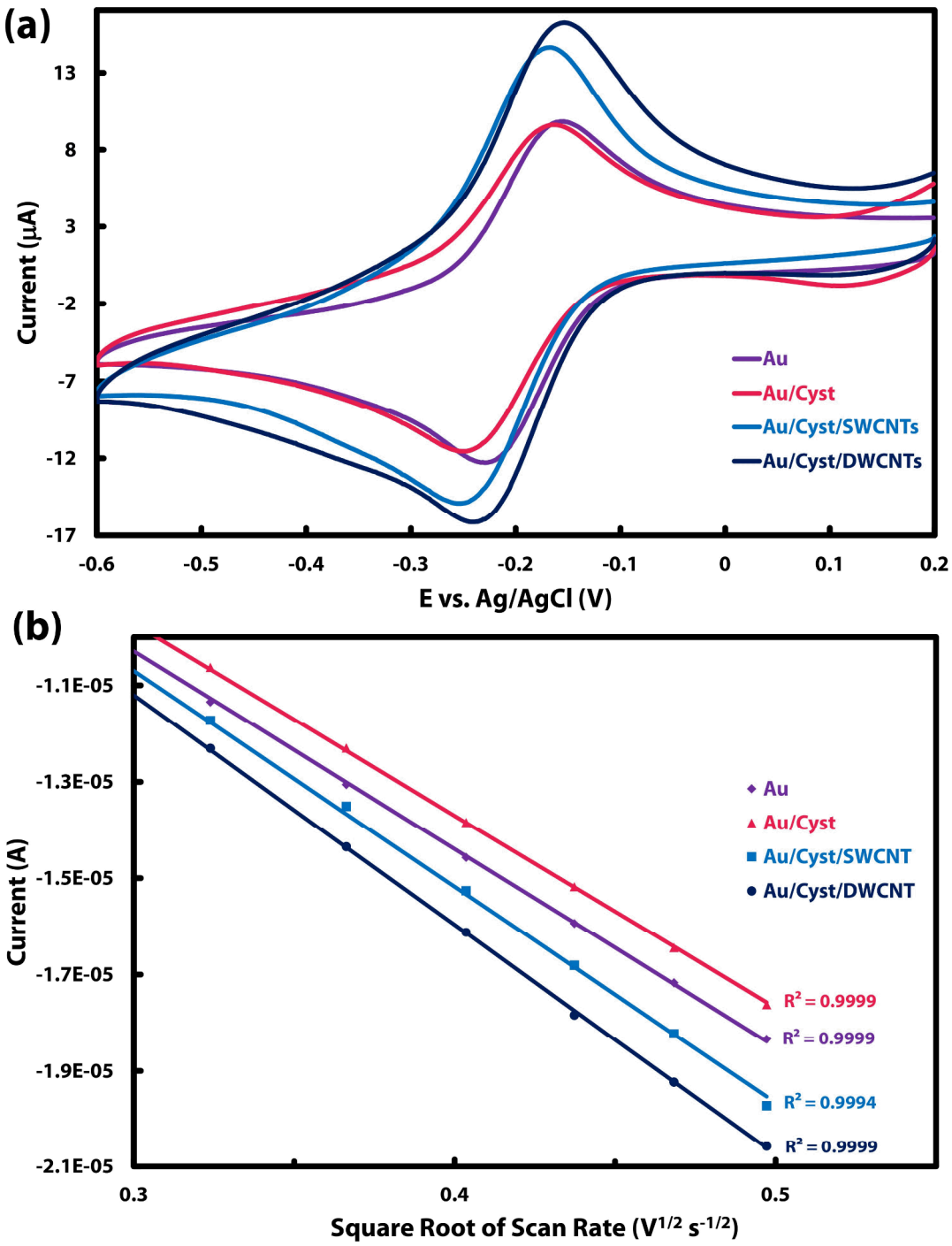

Figure 3 *(a) Cyclic voltammogram and (b) Randles-Sevcik plot of polished gold surfaces before and after addition of cysteamine and CNTs in 1 mM ruthenium hexaamine in potassium phosphate at a scan rate of 100 mV* s^{-1}.

Upon assembly of both SWCNTs and DWCNT the increase in electroactive area was calculated with use of the Randles-Sevcik equation.

$$i_P = \frac{0.447F^{3/2}An^{3/2}D^{1/2}Cv^{1/2}}{R^{1/2}T^{1/2}}$$

Where i_p is the peak current, n is the number of electrons involved in oxidation or reduction, A is the area of the working electrode (cm^2), D is the diffusion coefficient of the electroactive probe ($cm^2\ s^{-1}$) , C is the concentration of electroactive probe in the solution (mol cm^{-3}), and v, F, R and T have their usual significance. Diffusion rates for the oxidised and reduced species (D_O and D_R) are 5.71 x 10^{-7} $cm^2\ s^{-1}$ and 8.8 x 10^{-7} $cm^2\ s^{-1}$, respectively, as determined by Compton and co-workers [31].

Figure 3 (a) shows diffusion limited cyclic voltammograms of gold surfaces before and after addition of the cysteamine SAM and subsequent attachment of CNTs with $Ru(NH_3)_6^{+3/2}$ used as the redox probe. The reduction of ruthenium (III) to ruthenium (II) in aqueous solution involves the transfer of a single electron and exhibits close to ideal quasi-reversible outer sphere kinetic behaviour, making it a commonly used, fundamental redox reaction [8]. For a clean gold surface, the peak-to-peak potential (ΔE_p) was found to be 67 mV, and is comparable to the literature [32-34]. From the slope in Figure 3 (b) and the Randles-Sevcik equation, the electroactive area was calculated to be 5.72 ± 0.17 x 10^{-2} cm^2, which is slightly higher than the geometric area (3.14 x 10^{-2} cm^2) indicating the presence of surface roughness. After self-assembly of cysteamine a small decrease in current and an increase of ΔE_p to 87 mV is observed. The small reduction in current indicates that, despite the short chain length of the thiol, the cysteamine has increased resistance across the surface, slightly inhibiting electron transport to the underlying gold substrate. This has been shown in our previous work, where the addition of cysteamine resulted in a decrease of the apparent heterogeneous electron transfer rate of approximately 25% [24]. After the addition of CNTs, the ΔE_p is 82 mV for both CNT types and a significant increase in current is observed, particularly for the oxidation reaction. It has been shown by Gooding and co-workers that by adding conductive

nanoparticles to an insulating monolayer covered metal surface, the electron transfer properties can be 'switched on' again by enabling electron tunnelling through the insulating barrier [35]. Since the current after nanotube addition is significantly higher than that of the original gold surface, we conclude that the increased current is not simply a 'switching on' effect but demonstrates an increase in surface area has occurred. This is in agreement with our previous work showing atomic force microscopy images before and after CNT addition [24] where high aspect ratio features are clearly visible on the surface. From the measured peak currents the calculated surface areas are $8.04 \pm 0.14 \times 10^{-2}$ cm^2 and $6.13 \pm 0.18 \times 10^{-2}$ cm^2 for SWCNTs and DWCNTs, respectively. Therefore, modification with a cysteamine tether layer and subsequent addition of vertically aligned CNTs has enhanced the electrochemical properties of the gold electrode, by increasing the electroactive surface area.

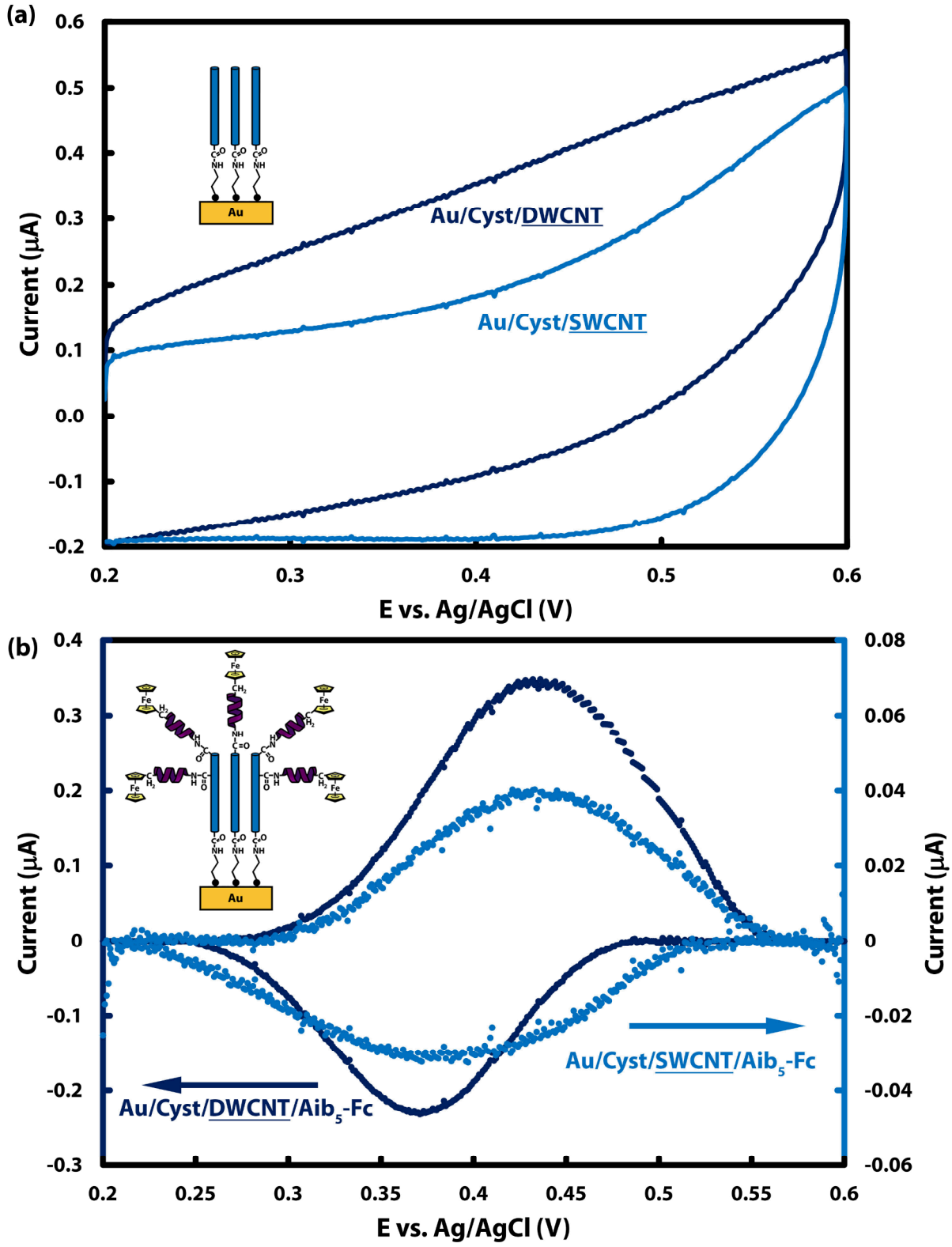

Figure 4 *Cyclic voltammograms of SWCNT and DWCNT electrode surfaces in 1 mM TBAPF6 in acetonitrile at a scan rate of 200 mV* s^{-1} *(a) before and (b) after functionalisation with* Aib_5*-Fc. (b) has been background subtracted.*

The electrochemical performance of both DWCNT and SWCNT electrodes before and after addition of Aib_5-Fc was then tested by cyclic voltammetry in TBAPF6/acetonitrile electrolyte solution. As can be seen in figure 4 (a) prior to the addition of Aib_5-Fc no redox peaks can be seen, and as a result of a large active surface area, a prominent capacitive background is observed. This is expected as both DWCNTs and SWCNTs are electrochemically inactive within the potential window from -0.6 V to 0.2 V. However after the surfaces were left in Aib_5-Fc solution containing peptide coupling agents for 48 h, oxidation and reduction peaks centred at 0.43 V and 0.37 V can be seen. Figure 4 (b) shows background subtracted scans at 200 mV s^{-1} for both DWCNT and SWCNT electrodes, where the left y-axis corresponds to the DWCNT and the right corresponds to the SWCNT. Immediately it can be seen that the DWCNT electrodes have a much higher peak current compared to its single walled counterpart with oxidative currents of 350 nA and 40 nA, respectively. Since both electrode surfaces have very similar topographies [24] this almost tenfold increase in current is attributed to a higher number of Aib_5-Fc redox protein bound to the nanotube walls. This is confirmed by calculation of the surface concentration of Aib_5-Fc molecules using Laviron's theory [30]. The surface concentration of Aib_5-Fc was determined to be $3.08 \pm 0.15 \times 10^{-11}$ mol cm^{-2} for the DWCNT electrode and $1.72 \pm 0.76 \times 10^{-11}$ mol cm^2 for the SWCNT electrode. This is expected due to the presence of significantly more carboxyl functionalities on the outer wall of a DWCNT compared to SWCNTs [23, 36]. This allows for greater attachment of the redox protein and a higher surface loading. These surface concentration values are comparable to previous work by Okamoto *et al.* who achieved a surface concentration of 4.7×10^{-11} mol cm^{-2} for triferrocene functionized double helix protein chains covalently bound to a gold surface by two thiol bonds [37]. Since Okamoto *et al.* used a flat gold surface for attachment of their peptides, it is expected that the CNT surface would achieve a much higher loading. However one must consider that each peptide used by

Okamoto *et al.* was bound with three ferrocene moieties, resulting in a higher surface concentration.

From Figure 4 (b), ΔE_p of the DWCNT and SWCNT electrodes are 65 mV and 37 mV, respectively. While the ideal ΔE_p should be zero for surface immobilized redox systems [30], these values still indicate very good electron transfer between the underlying gold substrate and the surface adsorbed redox protein. The non zero ΔE_p values observed for both types of CNTs can be attributed to the presence of a potential difference between the electrode and the redox centre, possibly formed by the electric double layer in the vertically aligned CNT array [38].

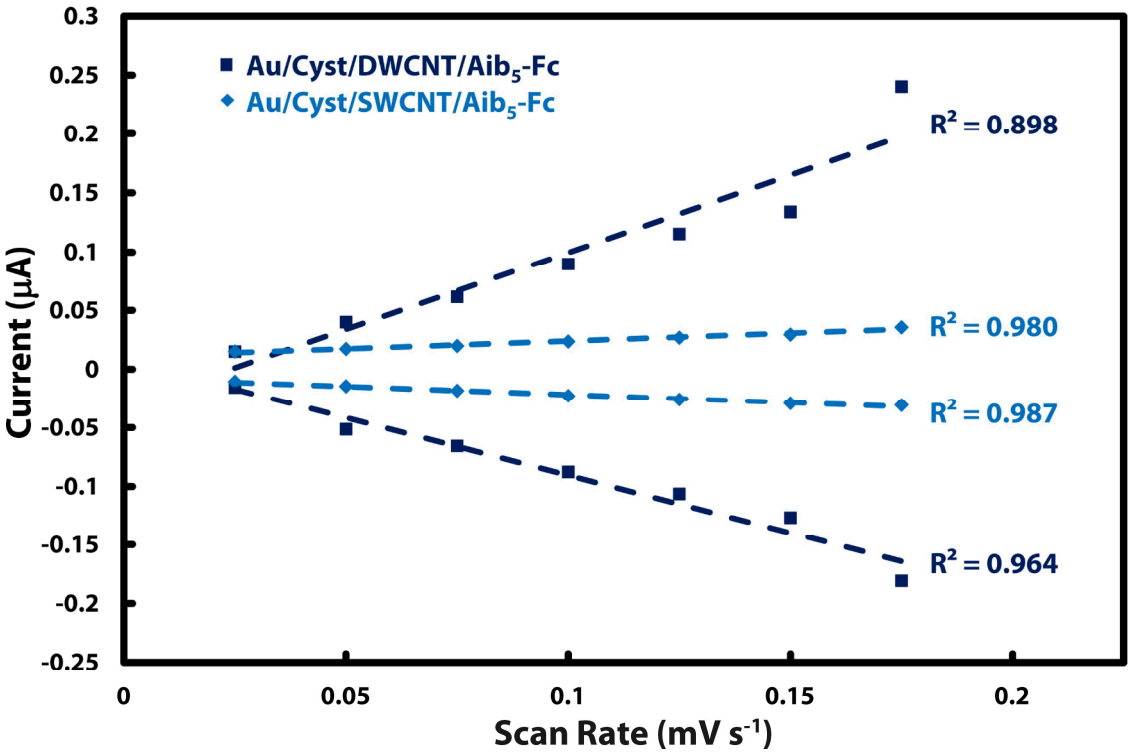

Figure 5 *Dependence of peak current on scan rate.*

The electrode kinetics for the Aib_5-Fc decorated CNT surfaces can be determined by plotting the oxidation and reduction peak currents against scan rate, as shown in Figure 5. It can be

seen that there is a clear linear relationship between the peak currents and the scan rate, which is indicative of surface bound electroactive species [39]. Furthermore, the slopes of the oxidation and reduction currents are symmetric around the origin, indicating that ΔE_p remains relatively constant with increasing scan rate.

The apparent electron transfer rate constants of the Aib_5-Fc decorated DWCNT and SWCNT were also calculated using Laviron's method for the condition of $\Delta E_p < 200/n$ mV. By considering the value of the transfer coefficient, α, to be between 0.3 and 0.7, the average electron transfer rates, k_{app}, were estimated according to the following equation.

$$k_{app} = \frac{mvnF}{RT}$$

where m is a dimensionless parameter related to the peak-to-peak separation. By using the slope from a plot of $v = f(m^{-1})$, mv could be determined and hence k_{app} found. The apparent electron transfer rate for the DWCNT and SWCNT electrodes were 31.6 ± 6.0 s^{-1}, and 23.3 ± 2.6 s^{-1}, respectively. Hence suggesting that an increased loading of redox protein was achieved without compromising the electron transfer capabilities. This suggests that electron transport in the DWCNTs occurs largely through the inner tube, since modification results in less disruption of the electronic transport capabilities.

4. Conclusion

The electron transfer properties of a ferrocene containing α-peptide adsorbed to DWCNT and SWCNT electrochemical surfaces was investigated. Due to the larger number of defects on the DWCNT outer walls, a higher surface concentration was achieved resulting in a higher electrochemical current. Determination of the apparent electron transfer rate showed this was at no expense to the DWCNT electron transfer capabilities. This result suggests that

DWCNT are advantageous to electrochemical surfaces as they can be chemically modified for attachment without compromising the electronic properties.

Acknowledgements

KM wishes to thank the Australian Government for an APA scholarship as well as the Playford Memorial Trust for a top up scholarship. This work is supported by the Australian Microscopy and Microanalysis Research Facility (AMMRF). B. S. Flavel gratefully acknowledges the support of the Alexander von Humboldt Foundation.

References

[1] M. Yang, Y. Yang, Y. Liu, G. Shen, R. Yu, Biosensors and Bioelectronics, 21 (2006) 1125-1131.
[2] S.K. Vashist, D. Zheng, K. Al-Rubeaan, J.H.T. Luong, F.-S. Sheu, Biotechnology Advances, 29 (2011) 169-188.
[3] C.B. Jacobs, M.J. Peairs, B.J. Venton, Analytica Chimica Acta, 662 (2010) 105-127.
[4] M. Delvaux, S. Demoustier-Champagne, Biosensors and Bioelectronics, 18 (2003) 943-951.
[5] J.J. Gooding, A. Chou, J. Liu, D. Losic, J.G. Shapter, D.B. Hibbert, Electrochemistry Communications, 9 (2007) 1677-1683.
[6] F. Berti, L. Lozzi, I. Palchetti, S. Santucci, G. Marrazza, Electrochimica Acta, 54 (2009) 5035-5041.
[7] J. Wang, Electroanalysis, 17 (2005) 7-14.
[8] L.Y. Heng, A. Chou, J. Yu, Y. Chen, J.J. Gooding, Electrochemistry Communications, 7 (2005) 1457-1462.
[9] S.H. Lim, J. Wei, J. Lin, Q. Li, J. KuaYou, Biosensors and Bioelectronics, 20 (2005) 2341-2346.
[10] X. Yu, B. Munge, V. Patel, G. Jensen, A. Bhirde, J.D. Gong, S.N. Kim, J. Gillespie, J.S. Gutkind, F. Papadimitrakopoulos, J.F. Rusling, Journal of the American Chemical Society, 128 (2006) 11199-11205.
[11] A. Venkatanarayanan, K. Crowley, E. Lestini, T.E. Keyes, J.F. Rusling, R.J. Forster, Biosensors and Bioelectronics, 31 (2012) 233-239.
[12] J.J. Gooding, R. Wibowo, J. Liu, W. Yand, S. Orbons, F.J. Mearns, J.G. Shapter, D.B. Hibbert, Journal of Ammerican Chemical Society, 125 (2003) 9006-9007.
[13] X. Guo, A.A. Gorodetsky, J. Hone, J.K. Barton, C. Nuckolls, Nat Nano, 3 (2008) 163-167.
[14] J. Yang, W.-D. Zhang, S. Gunasekaran, Biosensors and Bioelectronics, 26 (2010) 279-284.
[15] R. Somenath, V. Harindra, C. Wonbong, Nanotechnology, 17 (2006) S14.
[16] B. Flavel, M. Nambiar, J. Shapter, Silicon, (2011) 1-9.
[17] P. Diao, Z. Liu, Advanced Materials, 22 (2010) 1430-1449.
[18] M.W. Marshall, S. Popa-Nita, J.G. Shapter, Carbon, 44 (2006) 1137-1141.
[19] J. Yu, J.G. Shapter, J.S. Quinton, M.R. Johnston, D.A. Beattie, Physical Chemistry Chemical Physics, 9 (2006) 510-520.
[20] S. Banerjee, T. Hemraj-Benny, S.S. Wong, Advanced Materials, 17 (2005) 17-29.
[21] J. Zhao, H. Park, J. Han, J.P. Lu, The Journal of Physical Chemistry B, 108 (2004) 4227-4230.
[22] H. Matsumura, T. Ando, Journal of the Physical Society of Japan, 70 (2001) 2657-2665.
[23] K.E. Moore, B.S. Flavel, A.V. Ellis, J.G. Shapter, Carbon, 49 (2011) 2639-2647.
[24] K.E. Moore, B.S. Flavel, C.J. Shearer, A.V. Ellis, J.G. Shapter, Electrochemistry Communications, 13 (2011) 1190-1193.
[25] P.D. Beer, D.K. Smith, Journal of the Chemical Society-Dalton Transactions, (1998) 417.
[26] F. Ossola, P. Tomasin, F. Benetollo, E. Foresti, P.A. Vigato, Inorganica Chimica Acta, 353 (2003) 292-300.
[27] M.M. Walczak, D.D. Popenoe, R.S. Deinhammer, B.D. Lamp, C. Chung, M.D. Porter, Langmuir, 7 (1991) 2687-2693.
[28] M.J. Esplandiú, H. Hagenström, D.M. Kolb, Langmuir, 17 (2001) 828-838.

[29] M. Wirde, U. Gelius, L. Nyholm, Langmuir, 15 (1999) 6370-6378.
[30] E. Laviron, Journal of Electroanalytical Chemistry and Interfacial Electrochemistry, 101 (1979) 19-28.
[31] Y. Wang, J.G. Limon-Petersen, R.G. Compton, Journal of Electroanalytical Chemistry, 652 (2011) 13-17.
[32] H.O. Finklea, D.A. Snider, J. Fedyk, Langmuir, 6 (1990) 371-376.
[33] Q. Cheng, A. Brajter-Toth, Analytical Chemistry, 64 (1992) 1998-2000.
[34] S.E. Creager, D.M. Collard, M.A. Fox, Langmuir, 6 (1990) 1617-1620.
[35] J.B. Shein, L.M.H. Lai, P.K. Eggers, M.N. Paddon-Row, J.J. Gooding, Langmuir, 25 (2009) 11121-11128.
[36] A.H. Barber, R. Andrews, L.S. Schadler, H.D. Wagner, Applied Physics Letters, 87 (2005) 203106-203103.
[37] S. Okamoto, T. Morita, S. Kimura, Langmuir, 25 (2009) 3297-3304.
[38] I.M. Shiryaeva, J.P. Collman, R. Boulatov, C.J. Sunderland, Analytical Chemistry, 75 (2002) 494-502.
[39] M. Lyons, G. Keeley, Sensors, 6 (2006) 1791-1826.

Figure and Table Captions

Figure 1 *(a) The redox protein Aib_5-Fc and (b) fabrication of CNT electrodes decorated with covalently bound redox proteins.*

Figure 2 *Cyclic voltammetry cycle 1, 2 and 3 of a self assembled monolayer on polished gold in pH 6.5 potassium phosphate buffer, showing the irreversible oxidation of cysteamine at a scan rate of 100 mV s^{-1}.*

Figure 3 *(a) Cyclic voltammogram and (b) Randles-Sevcik plot of polished gold surfaces before and after addition of cysteamine and CNTs in 1 mM ruthenium hexaamine in potassium phosphate at a scan rate of 100 mV s^{-1}.*

Figure 4 *Cyclic voltammograms of SWCNT and DWCNT electrode surfaces in 1 mM TBAPF6 in acetonitrile at a scan rate of 200 mV s^{-1} (a) before and (b) after functionalisation with Aib_5-Fc. (b) has been background subtracted.*

Figure 5 *Dependence of peak current on scan rate.*